Interactions between atmospheric ultrafine particles and secondary organic aerosol mass: a model study

Erica R. Trump[1), Ilona Riipinen[1)2) and Neil M. Donahue[1)

[1) *Carnegie Mellon University, Center for Atmospheric Particle Studies, 1106 Doherty Hall, 5000 Forbes Avenue, Pittsburgh, PA, USA 15213*

[2) *Department of Applied Environmental Science and Bert Bolin Centre for Climate Research, Stockholm University, Svante Arrhenius väg 8, SE-114 18 Stockholm, Sweden*

Trump, E. R., Riipinen, I. & Donahue, N. M. 2014: Interactions between atmospheric ultrafine particles and secondary organic aerosol mass: a model study. *Boreal Env. Res.* 19: 352–362.

We use dynamic mass-balance equations to treat the role of organic composition in driving net condensation to atmospheric particles. We consider the growth of newly formed nanoparticles that may have very different composition (volatility) than the pre-existing aerosol. Production of vapors much less volatile than the background aerosol enhances the growth of nanoparticles by the re-partitioning of semi-volatile vapors to the growing nanoparticles. In contrast, production of more-volatile vapors suppresses the growth of nanoparticles because the background aerosol draws down the semi-volatile gas-phase concentrations. The background aerosol thus serves as either a source or a sink of additional organic material. For fresh nanoparticles, the implication is that net condensation depends significantly on any imbalance between the produced organic vapors and their equilibrium (vapor) distribution over the background aerosol. This phenomenon may be important during nucleation and growth events, where relatively rapid growth of newly formed particles is difficult to explain.

Introduction

Gas-particle partitioning is among the dominant physical processes controlling the size and composition of sub-micron (< 1 μm in diameter) atmospheric particulate matter. A large fraction of particulate nitrate, ammonium, and sulfate originates from the gas phase (Tsimpidi *et al.* 2007), and it has recently become clear that the same is true for an equally large fraction of organic aerosol (OA) (Donahue *et al.* 2009). While the partitioning of the inorganic species is relatively well understood (Nenes *et al.* 1998, Wexler and Clegg 2002), OA is another matter: it is comprised of a complex mixture of thousands of compounds having a wide range of volatilities (Marcolli *et al.* 2004, Robinson *et al.* 2010).

Organic compounds play an important role in the early stages of growth for nucleated particles (Riipinen *et al.* 2011). At the boreal forest site in Hyytiälä, Finland, for example, it is evident that the rate of particle growth is related to monoterpene concentrations (Hirsikko *et al.* 2005, Yli-Juuti *et al.* 2011); however, gas-phase production rates alone do not explain the magnitude of the observed particle growth rates (Riipinen *et al.* 2012). Processes such as organic salt formation and oligomerization likely explain part of this "missing" growth. Additionally, as we shall demonstrate, OA equilibration with the pre-ex-

isting aerosol likely enhances particle growth.

While gas-phase organic molecules constantly encounter particulate matter in the planetary boundary layer (Westervelt *et al.* 2013), only a fraction of those molecules contribute to net growth. Any net condensation to or evaporation from a particle is driven by deviations from thermodynamic equilibrium (Marcolli *et al.* 2004, Vehkamäki and Riipinen 2012). The final equilibrium state that the particle is trying to reach is characterized by the equilibrium concentrations (also expressed as vapor pressures) of the condensing or evaporating species in the particle and gas phases. The equilibrium concentration of an individual organic compound on a particle is controlled by the aerosol composition (the Raoult effect) as well as the curvature of the particle's surface (the Kelvin effect) (Seinfeld and Pandis 2006). These properties change dynamically during the course of the condensation process and vary significantly among particles in the atmosphere (Donahue *et al.* 2011). It is thus not at all obvious what part of the particle size distribution organic condensation will favor. Our objective was to investigate whether different conditions might lead to dramatically different organic condensational growth rates for nanoparticles.

Marcolli *et al.* (2004) showed that OA equilibration is accomplished via gas-phase diffusion and that the rate at which an organic species participates in equilibration depends on its volatility. This finding suggests that transfer of semi-volatile organics from the background aerosol to disequilibrated target particles ("Marcolli mixing") can be a key part of the equilibration process. The situation is especially dramatic for freshly formed or emitted nanoparticles that may have very different composition than the pre-existing background aerosol. The most extreme example is freshly emitted, completely uncoated nanoparticles. Consequently, we shall use these as an example of the general case by which particles evolve from a unique, external mixture to a homogenous internal mixture corresponding to the final equilibrium state.

In this work we applied a dynamic mass-transfer model (Vesala *et al.* 1997, Vehkamäki and Riipinen 2012) to treat the role of organic composition and particle size in driving the net condensation of semi-volatile organics to particles suspended in the atmosphere. We investigated the interactions between two aerosol populations: one consisting of freshly emitted ultrafine particles, and one representing the pre-existing background aerosol. Specifically, we investigated a situation in which the background aerosol consists of organics in the presence of additional sources of organic vapors — either from chemical aging reactions or direct emissions. We considered a monodisperse population of nanoparticles (representing the ultrafine particles) that is initially completely free of organic compounds and thus has a composition that is quite different from the background aerosol. We were interested in the net growth of those nanoparticles, specifically how the growth is influenced by the composition of the background particles as compared with the volatilities of the condensing vapors.

The composition (volatility) of condensing organics likely differs from the composition of the organics on the background aerosol particles, and this can have important implications for nanoparticle growth (Fig. 1). To demonstrate this phenomenology, we considered two limiting cases that represent conditions likely encountered in the atmosphere. In each case we introduced a source of organic vapors that leads to significant condensation onto and growth of the background aerosol; however, in one case the vapors are relatively less volatile than the equilibrium distribution that would normally exist over the background particles, while in the other case the vapors are relatively more volatile. The first case (less volatile vapors) is a reasonable model for gas-phase aging chemistry in the absence of fresh emissions (Lanz *et al.* 2007, Huffman *et al.* 2009). In this case the vapors can condense onto the nanoparticles and "prime" those particles to receive further condensation from more volatile organics associated with the background aerosol. The second case (more volatile vapors) is a reasonable model for "fresh" emissions in the presence of relatively aged background particles, which tend to be less volatile (Jimenez *et al.* 2009, Cappa and Jimenez 2010). When the new vapors are relatively volatile, the less-volatile background aerosol can serve as a sponge, preventing any significant condensation onto the nanoparticles.
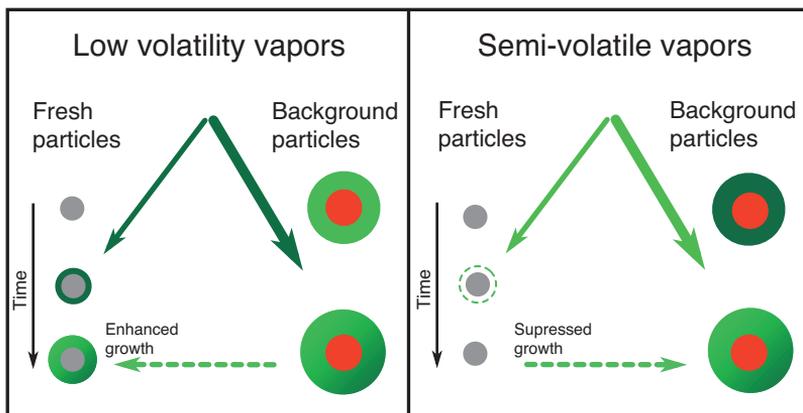
Fig. 1. Interaction of freshly formed particles with the pre-existing aerosol during organic condensation events. The background aerosol can serve to enhance growth if it contains relatively volatile organics. Conversely, a background aerosol containing relatively aged organics can serve to suppress the growth of newly formed particles.

Our results indicate that the interactions between emitted (fresh) nanoparticles and the background aerosol can strongly affect the amount of nanoparticle growth that occurs via reversible condensation of organics (the same compounds that form bulk secondary organic aerosol). Because the volatility of atmospheric organics varies over orders of magnitude, it is the volatility spread and not other effects such as particle curvature (the Kelvin effect) that dominate this behavior for all but the very smallest particles. Furthermore, we investigated how these condensation processes are influenced by the assumptions we make about the sizes and concentrations of the two particle populations.

Model description

We used the volatility basis set, introduced by Donahue *et al.* (2006), as a framework for describing the myriad of organic species found in the atmosphere. Organic species are grouped into logarithmically spaced bins based on their effective saturation concentration, or C^* (unit μg m^{-3}). Here, we treat each C^* bin as a lumped chemical species and describe the organic composition in terms of C^*. It is the difference in volatility between the organics constituting the background aerosol and the organics coating a fresh nanoparticle that drives the processes we shall describe.

We calculated the condensed mass for two distinct particle populations: a monodisperse nanoparticle mode consisting initially of non-volatile inorganic material and a larger-diameter background aerosol mode consisting of an organic mixture. The purpose of this study was not to model a specific set of ambient conditions, but rather to qualitatively demonstrate the influence of the background aerosol on nanoparticle growth. Nevertheless the population properties are roughly constrained based on an atmospheric size distribution from Hyytiälä (Riipinen *et al.* 2011). The Hyytiälä distribution (Fig. 2) contains a mode of freshly formed particles, which served as a basis for the monodisperse nanoparticle population. In our base case (Cases 1A–C), a population of 28-nm inorganic nanoparticles is introduced to an atmosphere containing a pre-existing background aerosol and in which vapor-phase emission occurs. We represent the background aerosol as a log-normal mode that initially consists of 50% organics by mass. This gives an initial background organic mass of 1.8 μg m^{-3}. We are not overly concerned about accurately representing the background size distribution; in these simulations the background aerosol serves as either a source or a sink of additional organic material depending on the conditions, as we shall demonstrate. To isolate the effect of condensation dynamics on the organic growth and composition of the ultrafine particles, we also omit other dynamic processes (such as coagulation and deposition) that would be shaping their distribution in the real atmosphere. The simulated environments contain vapor-phase organics that are initially in equilibrium with the background particles.

We represent the atmospheric organics as a mixture of "fresh" and "aged" components. In the real atmosphere this will include a broad
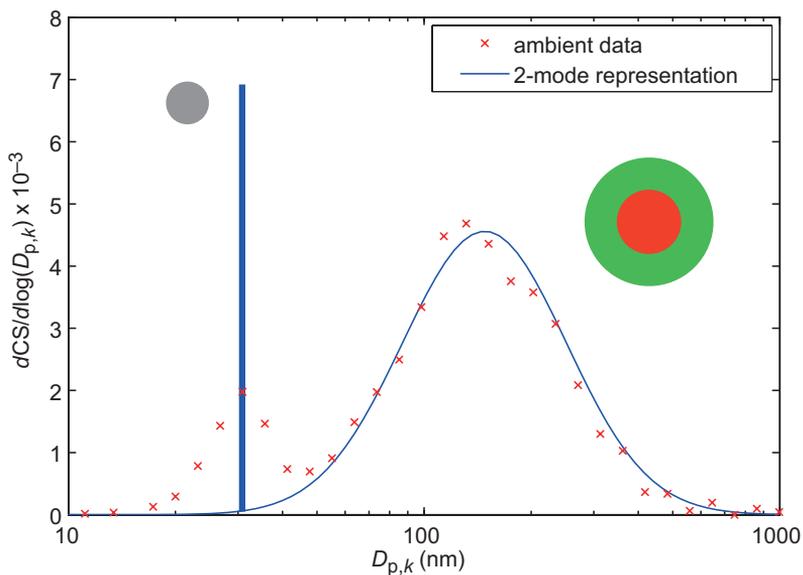
Fig. 2. The condensational sink, $d\text{CS}/d\log(D_{p,k})$ (s^{-1}), in an atmospheric aerosol distribution is shown (red points) along with its model representation (blue). The accumulation mode is represented as a lognormal particle distribution; the modeled nanoparticle mode is monodisperse.

distribution of volatilities (Cappa and Jimenez 2010), but to isolate the physics we reduce this to two constituents with volatilities differing by two orders of magnitude. For the fresh, relatively unoxidized (semi-volatile) organics, an effective saturation concentration of 1 μg m^{-3} ($\log_{10}C^* = 0$) is used; the C^* of the relatively aged, low-volatility organics is 0.01 μg m^{-3} ($\log_{10}C^* = -2$) (Jimenez *et al*. 2009). We assume that the fresh and aged organics exist in a single, well-mixed condensed phase (Koo *et al*. 2003, Hildebrandt *et al*. 2011) that is separate from and does not interact with the inorganic species (Pathak *et al*. 2008, Bertram *et al*. 2008). We do not explicitly represent the inorganic portion of the aerosol, as it would not substantially affect OA condensation in our simulations. Moreover, we do not describe the condensation of inorganic vapors that would contribute to nanoparticle growth in the real atmosphere. This representation of atmospheric species is greatly simplified, yet it is sufficient to illustrate the influence of organic composition on nanoparticle growth.

Organic vapors are added to the model atmosphere for the first three hours of the simulation; after this, the vapor production rate is instantaneously set to zero. The added vapors are "fresh" if they are less oxidized (more volatile) than the organics in the background atmosphere. Vapor-phase aging of organics may occur, resulting in

an effective influx of "aged" organic vapors; thus, the added vapors in this model are used as a proxy for either actual emissions or for gas-phase aging reactions resulting in lower-volatility vapors. We choose a vapor addition rate of 0.72 μg m^{-3} h^{-1} — this gives a growth rate of 10 nm h^{-1} for the background particles, which is roughly consistent with observed particle growth rates in Hyytiälä (Riipinen *et al*. 2011). Because organic production is less aggressive in many cases, we also consider vapor addition rates of 0.36 and 0.18 μg m^{-3} h^{-1}. We present these results as sensitivity studies (Cases 6A and C and 7A and C).

The ability of a nanoparticle to grow via organic condensation is dependent on the composition of particles in the background atmosphere. To illustrate this, we vary the volatility of the condensing vapor as compared with the volatility of the background aerosol. The "A" cases correspond to fresh condensing vapors, while the vapors in the "B" cases are relatively aged. In the "C" cases, both the added vapors and the background aerosol are aged. Furthermore, we study the sensitivity of the condensation process and the resulting nanoparticle growth rates to the properties of the two aerosol populations. We vary the diameter of the monodisperse nanoparticles to consider the growth of 10- and 60-nm particles (Cases 2A and B, and 3A and B). We also consider nanoparticle growth in the pres-

ence of background OA masses of 0.18 and 18 μg m^{-3} (Cases 4A and B, and 5A and B). Finally, we consider the growth of 10-nm nanoparticles using reduced vapor addition rates of 0.36 and 0.18 μg m^{-3} h^{-1} (Cases 8A and 9A). The assumed properties for the populations in each simulation are summarized in Table 1.

Model calculations

We use dynamic mass balance equations to predict the mass of each organic species in both particle populations (Eq. 1) as well as in the vapor phase (Eq. 2):

$$\frac{dC_{ij}^{\mathrm{p}}}{dt} = \Phi_{ij} \tag{1}$$

$$\frac{dC_{ii}^{\mathrm{vap}}}{dt} = P_i - \sum_j \phi_{ij} \tag{2}$$

In these equations, C_i represents the vapor (C_i^{vap}) or particulate (C_{ij}^{p}) phase concentration of species i (units μg m^{-3}), P_i is the rate of vapor-phase production (units μg m^{-3} s^{-1}), and Φ_{ij} is the net gas-to-particle mass transfer of species i to population j (units μg m^{-3} s^{-1}) (Seinfeld and Pandis 2006, Donahue *et al*. 2011). For an organic species:

$$\begin{aligned}\phi_{ij} &= \mathrm{CS}_j\left(C_i^{\mathrm{vap}} - C_{ij}^{\mathrm{surf}}\right)\\ &= \mathrm{CS}_j\left(C_i^{\mathrm{vap}} - X_{ij}C_i^*K_{\mathrm{e},j}\right)\\ &= \mathrm{CS}_jC_i^*\left(S_i - X_{ij}K_{\mathrm{e},j}\right)\end{aligned} \tag{3}$$

where CS_j is the condensation sink caused by the particle population j (units s^{-1}) (Dal Maso *et al*. 2002), C_{ij}^{surf} is the equilibrium concentration at the particle surface, which is the effective saturation concentration of a species modified by both the mass fraction of the species in the particle (X_{ij}) and the Kelvin term ($K_{\mathrm{e},j}$). The mass fraction accounts for thermodynamic mixing effects (modified Raoult's Law), the Kelvin term accounts for surface curvature effects, and S_i is the saturation ratio.

We approximate the Kelvin term for each particle population based on the modal diameter $D_{\mathrm{p},j}$. $K_{\mathrm{e},j}$ is also a function of the molar mass of the condensed species (M_i), particle temperature (T_{p}), average density of the condensed phase (ρ), the gas constant (R), and the surface tension of the condensed species (σ). We estimate the organic surface tension as $\sigma = 0.03$ N m^{-1} and write $K_{\mathrm{e},j}$ expressed in terms of a Kelvin diameter, D_{K}:

$$K_{\mathrm{e},j} = \exp\left(\frac{D_{\mathrm{K}}}{D_{\mathrm{p},j}}\right) \tag{4}$$

Table 1. Simulation descriptions and results

Case	Vapor addition rate (μg m^{-3} h^{-1})	Added organic ($\log_{10}C^*$)	Background organic ($\log_{10}C^*$)	Nanoparticle D_{p} (nm)	Initial OA in background (μg m^{-3})	Nanoparticle growth rate (nm h^{-1})
1A	0.72	−2	0	28	1.8	22
1B	0.72	0	−2	28	1.8	0
1C	0.72	−2	−2	28	1.8	10
2A	0.72	−2	0	10	1.8	18
2B	0.72	0	−2	10	1.8	0
3A	0.72	−2	0	60	1.8	22
3B	0.72	0	−2	60	1.8	0
4A	0.72	−2	0	28	0.18	35
4B	0.72	0	−2	28	0.18	0
5A	0.72	−2	0	28	18	6.7
5B	0.72	0	−2	28	18	0
6A	0.36	−2	0	28	1.8	18
6C	0.36	−2	−2	28	1.8	5.7
7A	0.18	−2	0	28	1.8	13
7C	0.18	−2	−2	28	1.8	2.8
8A	0.36	−2	0	10	1.8	13
9A	0.18	−2	0	10	1.8	6.2

$$D_{\text{K}} = \frac{2M_i\sigma}{RT_{\text{p}}\rho} \tag{5}$$

For an organic aerosol having a molecular weight of 200 g mol^{-1} and a density of 1.4 g cm^{-3}, $D_{\text{K}} = 7$ nm at 300 K (Donahue *et al.* 2011). Mass transfer to the background aerosol mode, which contains many particles having diameters greater than 100 nm, is thus not significantly affected by the Kelvin term. Moreover, because the driving force for organic condensation depends on $X \times K_{\text{e}}$, the growth rate of the nanoparticle mode, which has an organic composition that differs greatly from that of the background aerosol, is only weakly sensitive to the Kelvin term. However we shall explicitly explore this sensitivity by varying the diameter of the nanoparticle mode.

The condensation sink caused by particle population j is the loss frequency of vapors to the particle surface area:

$$\text{CS}_j = \sum_k N_k \frac{v_{\text{a}}}{4} \pi D_{\text{p},k}^2 \beta_k \tag{6}$$

where k refers to a particle size bin in a population j, N_k is the number concentration of particles in this bin, v_{a} is the mean thermal speed of the gas phase molecules, and β is the transition regime correction factor (Seinfeld and Pandis 2006):

$$\beta = \frac{2\alpha \text{Kn}(1 + \text{Kn})}{\text{Kn}^2 + \text{Kn} + 0.283\text{Kn}\alpha + 0.75\alpha} \tag{7}$$

As shown, β is a function of the accommodation coefficient (α) and the Knudsen number (Kn). Kn is a function of the mean free path of the organic vapor in air (λ_{AB}), which is generally defined as $3D_{\text{AB}}/v_{\text{a}}$ where D_{AB} is the diffusivity of A in air. For organic species, $\alpha = 1$ and $\lambda_{\text{AB}} = 100$ nm are used. We assume that the nanoparticle is coated perfectly (i.e., the mass accommodation coefficient of the "naked" nanoparticle is unity). The condensation sink sets the scaling for this mass transfer problem by establishing the collision rate of vapors with particles. We display an example of the differential condensation sink $d\text{CS}/d\log D_{\text{p},k}$ *vs.* $\log D_{\text{p},k}$ in an atmospheric size distribution to give a visual indication of which part of the particle size spectrum exhibits most molecular exchange with the gas phase (Fig. 2). We also indicate our model representation of the distribution. The distribution contains

a nucleation mode (centered at $D_{\text{p}} = 28$ nm) that is distinct from the background aerosol mode.

We consider the rate at which an initially inorganic nanoparticle would grow in the simulated environments (*see* Table 1). The growth is described by change in diameter (twice the rate at which any coating thickens), which is related to the mass flux to the particle:

$$\frac{dD_{\text{p},j}}{dt} = \frac{2J_j}{\rho \pi D_{\text{p},j}^2} \tag{8}$$

$$J_j = \sum_i \frac{\phi_{ij}}{N_j} \tag{9}$$

Here J_j is the average total molecular flux to a single particle in population j, $D_{\text{p},j}$ is the modal diameter of the population, and ρ is the average density of the condensing species. The molecular flux can also be formulated as the sum of the net condensation rates of each organic species to the monodisperse nanoparticle mode.

Our model explicitly tracks both the modal diameter (Eq. 9) and the total mass (Eq. 1) of both aerosol populations. However, we make simplifying assumptions regarding the background aerosol population in order to calculate CS using Eq. 6. These assumptions are that a) the particle size distribution remains log-normal throughout the simulation and that b) the geometric standard deviation of the lognormal distribution is constant at 1.74.

Results and discussion

Aged vapor emissions (Case 1A): Accelerated nanoparticle growth

This case represents an atmosphere having an influx of vapors that are aged relative to the background aerosol. The background aerosol in this case is semi-volatile ("SV-OOA", Jimenez *et al.* 2009), and the vapor influx may be caused by direct emission or by oxidation of background vapors. We show the time-dependent mass composition of the monodisperse nanoparticles (Fig. 3: 1A.1) and the background aerosol (Fig. 3: 1A.2), along with the vapor-phase concentrations of the organics, expressed in terms of saturation ratio (Fig. 3, subplot 1A.3). In this
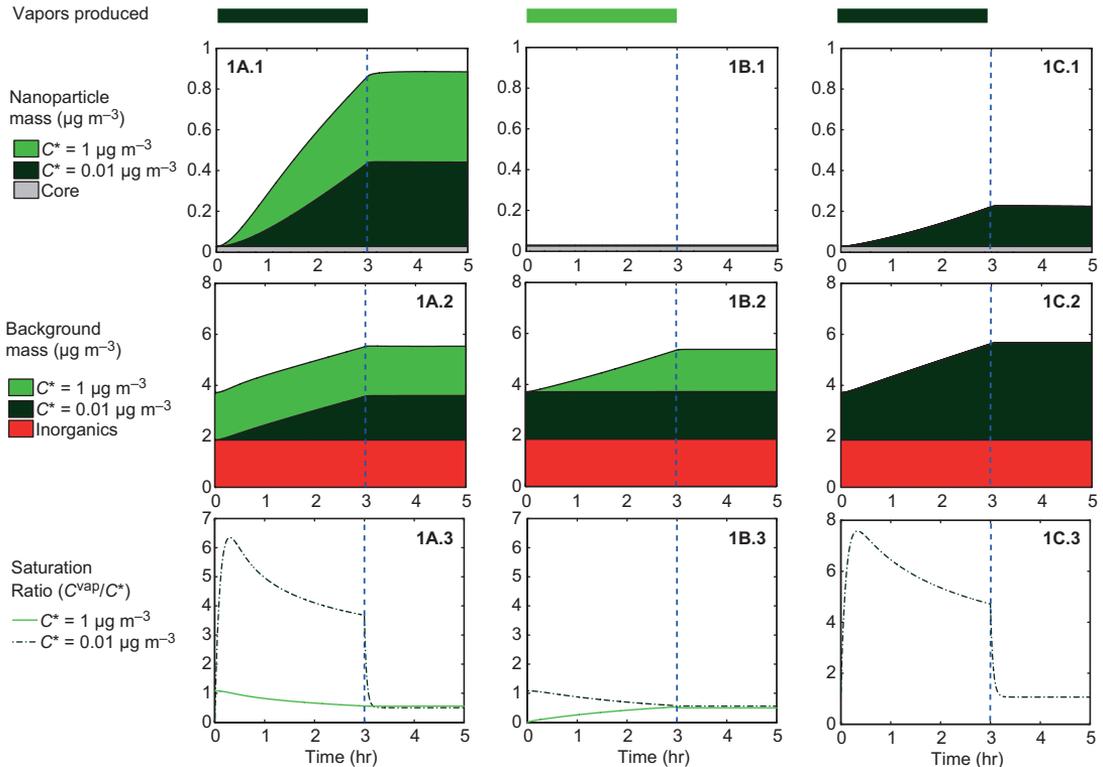
Fig. 3. The mass of the nanoparticle mode and the background mode (μg m^{-3}) is plotted against time for Cases 1A, 1B and 1C. In Case 1A low-volatility organics (dark green) are added to the simulation for three hours (dashed blue vertical line marks end of vapor production). Here the inorganic nanoparticles (grey) are coated with both low-volatility and semi-volatile (light green) organic species (subplot 1A.1). In Case 1B semi-volatile vapors are added to the simulation, and the inorganic nanoparticles are not coated (subplot 1B.1). In Case 1C low-volatility organics are added to the simulation and coat the nanoparticles. The evolution of the background particle mass (μg m^{-3}) and the vapor-phase saturation ratios are also shown for each respective case. The inorganic portion of the background particle mass is shown in red.

case aged organic vapors ($\log_{10}C^* = -2$) are added to a background atmosphere initially containing relatively volatile organics ($\log_{10}C^* = 0$). The vapor phase is very quickly saturated with the aged organics ($S_i > C^* \times X_i \times K_e$, *see* Eq. 3) and growth begins as vapors condense onto both the background aerosol and the bare nanoparticles. When the aged organics begin to condense, the composition of the background aerosol is essentially unchanged ($X_{\log 10 C^* = -2} \sim 0$), while the organic portion of the nanoparticles is comprised entirely of low-volatility organics ($X_{\log 10 C^* = -2} = 1$). As a consequence, the equilibrium mass concentration of semi-volatile ($\log_{10}C^* = 0$) vapors over the nanoparticles is essentially zero while over the background aerosol it is 1 μg m^{-3}. There is thus a strong driving force for additional condensation to the nanoparticles, while the back-

ground aerosol serves as a reservoir to maintain the semi-volatile vapor concentration. This leads to substantially enhanced nanoparticle growth (*see* Fig. 4). Case 1C (also shown in Fig. 3) shows the nanoparticle growth rate in absence of this composition driving force; the enhancement for Case 1A is a factor of two (22 nm h^{-1} *vs.* 10 nm h^{-1}). If some portion of the background organic mass is characterized by delayed evaporation, whether due to slow decomposition of oligomers or to diffusive limitations, the growth rate is somewhere in between (14 nm h^{-1} when 50% of background is effectively non-volatile).

In Case 1A the organics condense very quickly, bringing the compositions of the two particle populations into balance. As vapor-phase emission continues, additional $\log_{10}C^* = 0$ and $\log_{10}C^* = -2$ vapors condense in propor-

tion to their equilibrium concentrations. In Case 1A, 2.2 μg m^{-3} of low-volatility organics are produced, with 80% condensing onto the background particles. An additional 0.48 μg m^{-3} of semi-volatile ($\log_{10}C^* = 0$) vapors re-partition to the condensed phase, with 85% condensing onto the nanoparticles. The partitioning thermodynamics directs this additional condensation preferentially to the nanoparticles.

One situation where this phenomenon may be important is during nucleation and growth events, where relatively rapid growth of newly formed particles is difficult to explain (Donahue *et al*. 2011, Riipinen *et al*. 2011, Pierce *et al*. 2011). In that case, the nanoparticles in this simulation are the nucleated particles in the atmosphere, and the low-C^* vapors are produced via gas-phase oxidation.

Aged background aerosol (Case 1B): Inhibited nanoparticle growth

The background aerosol in this is less volatile (lower C^*) than the added vapors. This case represents an atmosphere that is characterized by fresh, relatively unoxidized vapors and a relatively aged (and therefore less volatile) background aerosol ("LV-OOA", Jimenez *et al*. 2009). Here, organic condensation does not cause the nanoparticle population to grow; this is true even though significant OA is formed via gas-particle partitioning (the total amount of OA produced is comparable to Case 1A, as shown in Fig. 3). The added $\log_{10}C^* = 0$ organics do interact with the nanoparticles; however, because the molecules are relatively volatile they do not remain condensed on the particle. Rather, the semi-volatile organics are free to distribute amongst particle populations in the most thermodynamically favorable way. In this case, that is almost exclusively deposition to the background aerosol. Because the background initially contains lower-volatility organics, $X_{\log10C^*=0}$ remains low enough in the background aerosol to keep the equilibrium mass concentration of the $\log_{10}C^* = 0$ vapors relatively low; this drives condensation toward the background aerosol throughout the simulation and sharply reduces any net condensation to the nanoparticles. Because this driving
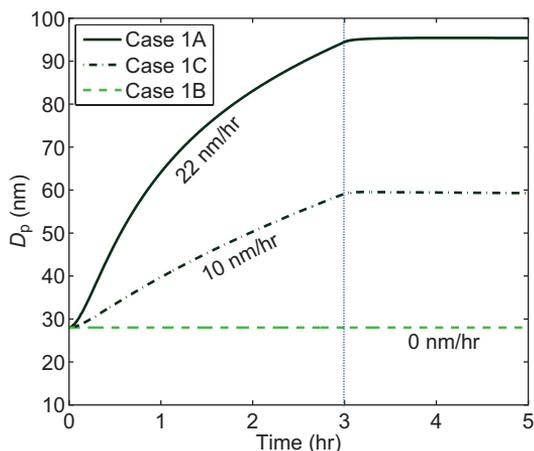
Fig. 4. The condensational growth of the monodisperse nanoparticle mode is shown for three sets of conditions. In Case 1A the nanoparticles grow (22 nm h^{-1}) as the added low-volatility vapors condense; the growth is enhanced by relatively volatile organics from the background atmosphere that selectively condense onto the nanoparticles. The nanoparticles in Case 1C also grow (10 nm h^{-1}) as low-volatility vapors condense. In Case 1B the nanoparticles do not grow. The blue vertical line marks end of vapor production.

force exists, and because the condensation sink of the background aerosol is sufficiently high, the background aerosol absorbs almost all of the added $\log_{10}C^* = 0$ vapors (*see* Fig. 3, subplots 1B.1 and 1B.2). As shown, the growth of the nanoparticle mode is extremely limited (Fig. 4).

Sensitivity studies

We explore the sensitivity of our results to nanoparticle size (and thus the Kelvin effect) by varying the initial diameter of the monodisperse mode. In addition to the base-case ($D_p = 28$ nm), we consider modes having initial diameters of 10 and 60 nm. As summarized (Table 1), the calculated nanoparticle growth rates are rather insensitive to the initial particle size. In all cases having relatively aged added vapors, the growth of the nanoparticle mode is rapid; and when the background is relatively aged, the nanoparticle mode does not grow. In Case 2A (10 nm nanoparticles, aged vapors), the nanoparticle growth rate is slightly lower than the growth rate for the nanoparticles in the corresponding base-case

simulation (Case 1A). This is because a higher saturation ratio is required to drive initial condensation to the nanoparticle mode.

We also explore the sensitivity of our results to the initial mass of the background OA by varying the mass over two orders of magnitude (we consider background OA mass of 0.18, 1.8, and 18 μg m^{-3}). In all cases having relatively aged added vapors, the nanoparticle mode grows; however, its growth rate depends on the mass concentration of the background OA. When the magnitude of the background OA mode is increased (Case 5A), the background receives a greater fraction of the OA condensation, resulting in reduced growth for the nanoparticle mode relative to Case 1A. The nanoparticle mode does not grow in any of the cases having a relatively aged background OA.

We further consider the sensitivity of our results to the vapor production rate (we consider rates of 0.18 μg m^{-3} h^{-1}, 0.36 μg m^{-3} h^{-1}, and 0.72 μg m^{-3} h^{-1}). All of the associated "A" cases exhibit nanoparticle growth that is enhanced by the presence of the background aerosol population. The enhancement factors for the lower production rates are 3 and 5 (corresponding to Cases 6A and C, and 7A and C, respectively). For lower production rates, greater amounts of semi-volatile organics must transfer to the nanoparticles in order to equilibrate the population with the background aerosol. Finally, we consider sensitivity to particle size when the organic production rate is reduced (Cases 8A and 9A). We find that organics contribute to the growth of 10-nm particles at the given production rates.

Conclusions

These simulations are not designed to model the real atmosphere but rather to illuminate the underlying physics driving net condensation of organics over a complex mixture. However, as long as the equilibrium thermodynamics at the heart of all partitioning treatments of organic aerosol is valid, the essential dynamics described here will have an important role in organic condensation onto atmospheric particles. The essential feature is that composition differences can drive substantial net fluxes onto or off of different particles, so that net growth may be quite different than for the relatively simple case of an essentially non-volatile gas-phase species like sulfuric acid.

For fresh nanoparticles, the implication is that coating will depend significantly on any imbalance between the produced organic vapors and their equilibrium (vapor) distribution over the bulk background organic aerosol, which is generally in the accumulation mode. There is strong evidence for gas-phase production of at least some very low volatility organics, so it is likely that situations similar to Case 1A will be frequently encountered in the atmosphere. Our results indicate that the growth rate of nanoparticles having $D_p > 10$ nm may be enhanced due to vapor-phase equilibration of the nanoparticles with the background atmosphere. However, these simulations also show that the enhancements depend strongly on the volatility difference between the condensing vapors being produced in the gas phase and the compounds in the background aerosol; thus, whether condensation proceeds as "semi-volatile", "non-volatile" or even "enhanced" will depend on the specific conditions during an event. Nonetheless, the "enhanced" condensation caused by transfer of semi-volatile material from the accumulation mode could help to explain observed nanoparticle growth rates and should thus be considered when studying the organic contribution to nanoparticle growth.

References

Bertram A.K., Martin S.T., Hanna S.J., Smith M.L., Bodsworth A., Chen Q., Kuwata M., Liu A., You Y. & Zorn S.R. 2011. Predicting the relative humidities of liquid-liquid phase separation, efflorescence, and deliquescence of mixed particles of ammonium sulfate, organic material, and water using the organic-to-sulfate mass ratio of the particle and the oxygen-to-carbon elemental ratio of the organic component. *Atmos. Chem. Phys.* 11: 10995–11006.

Cappa C.D. & Jimenez J.L. 2010. Quantitative estimates of

the volatility of ambient organic aerosol. *Atmos. Chem. Phys.* 10: 5409–5424.

Dal Maso M., Kulmala M., Lehtinen K.E.J., Mäkelä J.M., Aalto P. & O'Dowd C.D. 2002. Condensation and coagulation sinks and formation of nucleation mode particles in coastal and boreal forest boundary layers. *J. Geophys. Res.* 107, 8097, doi 10.1029/2001jd001053.

Donahue N.M., Robinson A.L., Stanier C.O. & Pandis S.N. 2006. Coupled partitioning, dilution, and chemical aging of semivolatile organics. *Environ. Sci. Technol.* 40: 2635–2643.

Donahue N.M., Robinson A.L. & Pandis S.N. 2009. Atmospheric organic particulate matter: from smoke to secondary organic aerosol. *Atmos. Environ.* 43: 94–106.

Donahue N.M., Trump E.R., Pierce J.R. & Riipinen I. 2011. Theoretical constraints on pure vapor-pressure driven condensation of organics to ultrafine particles. *Geophys. Res. Lett.* 38, L16801, doi 10.1029/2011gl048115.

Hildebrandt L., Henry K.M., Kroll J.H., Worsnop D.R., Pandis S.N. & Donahue N.M. 2011. Evaluating the mixing of organic aerosol components using high-resolution aerosol mass spectrometry. *Environ. Sci. Technol.* 45: 6329–6335.

Hirsikko A., Laakso L., Horrak U., Aalto P.P., Kerminen V.M. & Kulmala M. 2005. Annual and size dependent variation of growth rates and ion concentrations in boreal forest. *Boreal Env. Res.* 10: 357–369.

Huffman J.A., Docherty K.S., Aiken A.C., Cubison M.J., Ulbrich I.M., DeCarlo P.F., Sueper D., Jayne J.T., Worsnop D.R., Ziemann P.J. & Jimenez J.L. 2009. Chemically-resolved aerosol volatility measurements from two megacity field studies. *Atmos. Chem. Phys.* 9: 7161–7182.

Jimenez J.L., Canagaratna M.R., Donahue N.M., Prevot A.S.H., Zhang Q., Kroll J.H., DeCarlo P.F., Allan J.D., Coe H., Ng N.L., Aiken A.C., Docherty K.S., Ulbrich I.M., Grieshop A.P., Robinson A.L., Duplissy J., Smith J.D., Wilson K.R., Lanz V.A., Hueglin C., Sun Y.L., Tian J., Laaksonen A., Raatikainen T., Rautiainen J., Vaattovaara P., Ehn M., Kulmala M., Tomlinson J.M., Collins D.R., Cubison M.J., Dunlea E.J., Huffman J.A., Onasch T.B., Alfarra M.R., Williams P.I., Bower K., Kondo Y., Schneider J., Drewnick F., Borrmann S., Weimer S., Demerjian K., Salcedo D., Cottrell L., Griffin R., Takami A., Miyoshi T., Hatakeyama S., Shimono A., Sun J.Y., Zhang Y.M., Dzepina K., Kimmel J.R., Sueper D., Jayne J.T., Herndon S.C., Trimborn A.M., Williams L.R., Wood E.C., Middlebrook A.M., Kolb C.E., Baltensperger U. & Worsnop D.R. 2009. Evolution of Organic Aerosols in the Atmosphere. *Science* 326: 1525–1529.

Koo B.Y., Ansari A.S. & Pandis S.N. 2003. Integrated approaches to modeling the organic and inorganic atmospheric aerosol components. Atmos. Environ. 37: 4757–4768.

Lanz V.A., Alfarra M.R., Baltensperger U., Buchmann B., Hueglin C. & Prevot A.S.H. 2007. Source apportionment of submicron organic aerosols at an urban site by factor analytical modelling of aerosol mass spectra. *Atmos. Chem. Phys.* 7: 1503–1522.

Marcolli C., Luo B.P., Peter T. & Wienhold F.G. 2004. Inter-

nal mixing of the organic aerosol by gas phase diffusion of semivolatile organic compounds. *Atmos. Chem. Phys.* 4: 2593–2599.

Nenes A., Pandis S.N. & Pilinis C. 1998. ISORROPIA: a new thermodynamic equilibrium model for multiphase multicomponent inorganic aerosols. *Aquat. Geochem.* 4: 123–152.

Pathak R., Donahue N.M. & Pandis S.N. 2008. Ozonolysis of beta-pinene: Temperature dependence of secondary organic aerosol mass fraction. *Environ. Sci. Technol.* 42: 5081–5086.

Pierce J.R., Riipinen I., Kulmala M., Ehn M., Petaja T., Junninen H., Worsnop D.R. & Donahue N.M. 2011. Quantification of the volatility of secondary organic compounds in ultrafine particles during nucleation events. *Atmos. Chem. Phys.* 11: 9019–9036.

Riipinen I., Pierce J.R., Yli-Juuti T., Nieminen T., Hakkinen S., Ehn M., Junninen H., Lehtipalo K., Petaja T., Slowik J., Chang R., Shantz N.C., Abbatt J., Leaitch W.R., Kerminen V.-M., Worsnop D.R., Pandis S.N., Donahue N.M. & Kulmala M. 2011. Organic condensation: a vital link connecting aerosol formation to cloud condensation nuclei (CCN) concentrations. *Atmos. Chem. Phys.* 11: 3865–3878.

Riipinen I., Yli-Juuti T., Pierce J.R., Petaja T., Worsnop D.R., Kulmala M. & Donahue N.M. 2012. The contribution of organics to atmospheric nanoparticle growth. *Nature Geosci.* 5: 453–458.

Robinson A.L., Grieshop A.P., Donahue N.M. & Hunt S.W. 2010. Updating the Conceptual Model for Fine Particle Mass Emissions from Combustion Systems. *J. Air & Waste Manage. Assoc.* 60: 1204–1222.

Seinfeld J.H. & Pandis S.N. 2006. *Atmospheric chemistry and physics — from air pollution to climate change*, 2nd ed. John Wiley & Sons, New York.

Tsimpidi A.P., Karydis V.A. & Pandis S.N. 2007. Response of inorganic fine particulate matter to emission changes of sulfur dioxide and ammonia: The eastern United States as a case study. *J. Air Waste Manage. Assoc.* 57: 1489–1498.

Vehkamäki H. & Riipinen I. 2012 Thermodynamics and kinetics of atmospheric aerosol particle formation and growth. *Chem. Soc. Rev.* 41: 5160–5173.

Vesala T., Kulmala M., Rudolf R., Vrtala A. & Wagner P.E. 1997. Models for condensational growth and evaporation of binary aerosol particles. *J. Aerosol Sci.* 28: 565–598.

Westervelt D.M., Pierce J.R., Riipinen I., Trivitayanurak W., Hamed A., Kulmala M., Laaksonen A., Decesari S. & Adams P.J. 2013. Formation and growth of nucleated particles into cloud condensation nuclei: model–measurement comparison. *Atmos. Chem. Phys.* 13: 7645–7663.

Wexler A.S. & Clegg S.L. 2002. Atmospheric aerosol models for systems including the ions H^+, NH_4^+, Na^+, SO_4^{2-}, NO_3^-, Cl^-, Br^-, and H_2O. *J. Geophys. Res.* 107, 4207, doi 10.1029/2001jd000451.

Yli-Juuti T., Nieminen T., Hirsikko A., Aalto P.P., Asmi E., Horrak U., Manninen H.E., Patokoski J., Dal Maso M., Petaja T., Rinne J., Kulmala M. & Riipinen I. 2011.

Growth rates of nucleation mode particles in Hyytiala during 2003–2009: variation with particle size, season, data analysis method and ambient conditions. *Atmos. Chem. Phys.* 11: 12865–12886.